JMEPEG (2005) 14:75-84
DOI: 10.1361/10599490522347

1059-9495/$19.00

Effect of Ion Nitriding on the Abrasive Wear Resistance of Ultrahigh-Strength Steels with Different Silicon Contents

R.M. Muñoz Riofano, L.C. Casteletti, and P.A.P. Nascente

(Submitted February 17, 2005)

This article studies the effect of silicon (Si) on ultrahigh-strength AISI 4340 steels in connection with the thermal treatment, as well as the influence of this element on nitriding and, consequently, abrasive wear. Four alloys with different Si contents were nitrided at 350 °C (4 and 8 h) and 500 and 550 °C (2 and 4 h) in a gas mixture of 80 vol.% H_2 and 20 vol.% N_2. The nitrided layers were characterized by microhardness and pin-on-disk tests, optical microscopy, scanning electron microscopy with energy-dispersive x-ray spectrometry, and x-ray diffraction (XRD). The increase in Si enhanced the tempering resistance of the steels and also improved considerably the hardness of the nitrided layers. The increase in Si produced thinner compound layers with better hardness quality and high abrasive wear resistance. XRD analysis detected a mixture of nitrides in the layers γ'-Fe_4N, ε-$Fe_{2\text{-}3}N$, CrN, MoN, and Si_3N_4 with their proportions varying with the nitriding conditions.

Keywords abrasive wear, ion nitriding, silicon, ultrahigh-strength steel

1. Introduction

The ultrahigh-strength steels are technologically well established, being used in several applications, mainly in the mechanical and aerospace industries. AISI 4340 steel is considered to be the standard to which other ultrahigh-strength steels are compared (Ref 1). This steel is used in the quenched and tempered states to reach a better combination of mechanical strength, ductility, and toughness. However, in certain circumstances, as in the case of components subjected to severe wear, it is necessary to enhance its surface properties. Among the surface-hardening techniques used, ion nitriding has proven to be a good candidate for treating ultrahigh-strength steels, because the parts are less susceptible to distortions, as can occur in other conventional surface treatments. Ion nitriding permits adequate control of the formed layer with metallurgical properties suitable for several service conditions (Ref 2-5). In addition to this, ion nitriding allows for relatively low-temperature treatments (i.e., close to 350 °C) without causing tempering embrittlement in the substrate (Ref 6). It is important to understand the material behavior during nitriding because the treatment temperature will also cause tempering of the substrate.

Ion nitriding is a thermochemical process for surface hardening that employs an electric discharge in gases, producing plasma, which permits the interstitial insertion of nitrogen (N) into the substrate lattice. Nitrogen reacts with iron and other alloying elements in the steel surface, forming an external layer, which is denoted as the compound layer, with the further diffusion of N into the substrate (diffusion zone). The alloying elements (e.g., Cr, Al, Ti, Si, Mo, V, Mn, and W) present in the steels are of fundamental importance, because they will determine the kind and behavior of the nitrided layer, because they are elements that form the nitrides (Ref 7-9). The compound layer and the diffusion zone improve surface hardness, wear and fatigue resistance, the friction coefficient, and corrosion and oxidation resistance. For better service performance in engineering applications, it is crucial to control nitride layer formation and thickness, which can be achieved by controlling the

R.M. Muñoz Riofano and **L.C. Casteletti,** Departamento de Engenharia de Materiais, Aeronáutica e Automobilística, Escola de Engenharia de São Carlos, Universidade de São Paulo, Av. Trabalhador São-Carlense 400, São Carlos, SP 13566-590, Brazil; and **P.A.P. Nascente,** Departamento de Engenharia de Materiais, Universidade Federal de São Carlos, São Carlos, SP 13656-905, Brazil. Contact e-mail: nascente@power.ufscar.br.

Table 1 Nominal chemical compositions of modified 4340

	Composition, wt.%						
Alloy	C	Si	Cr	Ni	Mo	Mn	Fe
L1	0.44	0.69	0.87	1.78	0.27	0.77	bal
L2	0.43	1.32	0.87	1.77	0.27	0.78	bal
L3	0.43	1.61	0.88	1.77	0.27	0.78	bal
L4	0.41	1.89	0.88	1.75	0.43	0.79	bal

Table 2 Measured chemical compositions of alloys

	Composition, wt.%						
Alloy	C	Si	Cr	Ni	Mo	Mn	Fe
L1	0.42	0.62	0.92	2.18	0.28	0.85	bal
L2	0.41	1.27	0.86	2.15	0.28	0.84	bal
L3	0.43	1.68	0.88	2.14	0.29	0.82	bal
L4	0.40	1.98	0.89	2.10	0.50	0.77	bal

nitriding parameters, and this versatility is one of the main characteristics of the process.

The objective of this work was the verification of the effect of silicon (Si) on ultrahigh-strength, ion-nitrided AISI 4340 steels. The characteristics of the nitrided layers were investigated, as well as their wear resistance, as a function of treatment temperature and time.

2. Experimental Procedures

Four alloys with modified AISI 4340 steel composition were produced (Table 1). The alloys with different Si contents were melted in a vacuum-induction furnace and then cast in the shape of round bars in a sand mold according to the ASTM standard (Ref 10). Each alloy was identified by a code related to the Si content: L1, 0.69% Si; L2, 1.32% Si; L3, 1.61% Si; and L4, 1.89% Si.

Table 3 Effect of Si content and tempering time on alloy hardness

	Vickers hardness, HV		
Alloy	Tempered for 1 h	Tempered for 3 h	Tempered for 5 h
L1	436	419	410
L2	485	459	458
L3	503	482	470
L4	534	514	493

The samples were machined into a cylindrical shape, having a diameter of 10 mm and a length of 10 mm. The cylindrical samples were austenitized at 850 °C for 2.5 h, oil quenched with agitation, and tempered at 550 °C for 1, 3, and 5 h. The tempered samples were identified by codes: 1R (1 h), 3R (3 h) and 5R (5 h).

The surface preparation involved grinding one of the sample faces on 80 to 1200 mesh, polishing it on 0.3 and 0.05 μm alumina abrasives, and ultrasonic cleaning with petroleum ether for 12 min. The ion nitriding was carried out using a cylindrical stainless steel reactor with a diameter and height of 300 mm. The power source provided a maximum voltage of 800 V and continuous current with power of 2 kVA. The nitriding temperatures were 350 °C (4 and 8 h), and 500 °C, and 550 °C (2 and 4 h). For all treatments a gas mixture of 80 vol.% H_2 and 20 vol.% N_2 under a pressure of 5 mbar was used. After nitriding, the samples were cooled in a vacuum.

Following the nitriding procedure, the samples were cross sectioned for metallographic observations and microhardness tests. The metallographic preparation consisted of grinding on

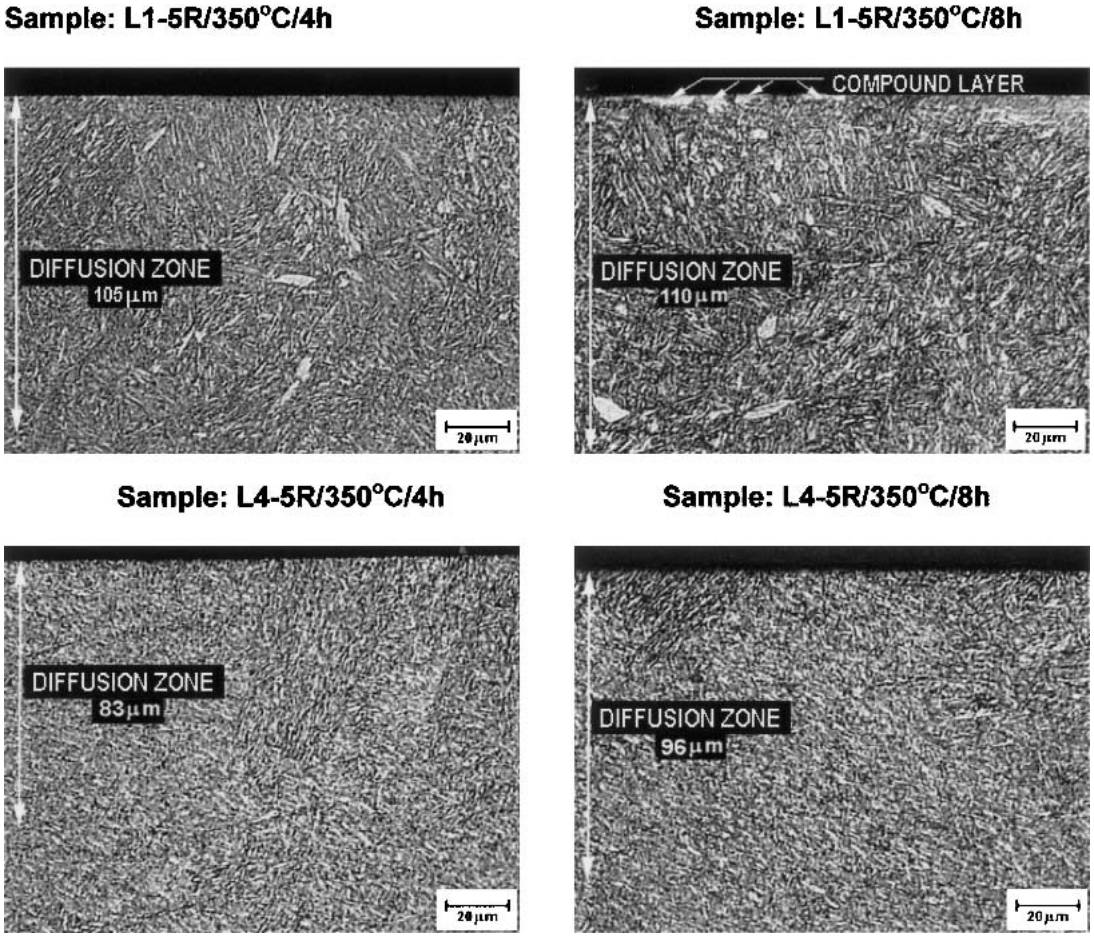

Fig. 1 Optical micrographs of the L1 and L2 alloys tempered for 5 h and ion nitrided at 350 °C for 4 and 8 h

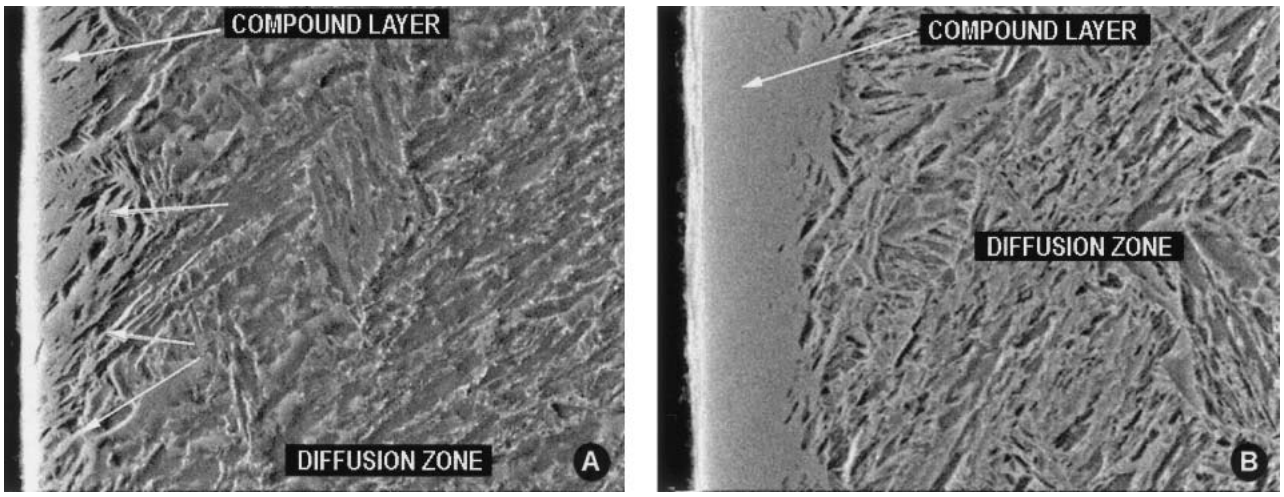

Fig. 2 SEM micrographs of the nitrided layers for (a) the L4-3R/500 °C/2 h sample and (b) the L4-3R/500 °C/4 h sample showing the compound layer

Table 4 Depth of the nitrided layers

	Layer thickness, μm										
	350 °C/ 4 h	350 °C/ 8 h		500 °C/ 2 h		500 °C/ 4 h		550 °C/2 h		550 °C/4 h	
Alloy	CN	CN	CC	CN	CC	CN	CC	CN	CC + SC	CN	CC + SC
L1-1R	84	109	3	102	4.8	165	5.8	151	12.1	173	7.2 + 13.7 = 20.9
L2-1R	83	106	…	93	4.4	130	5.8	134	11.4	142	6.5 + 11.1 = 17.6
L3-1R	76	92	…	84	3.9	121	4.6	121	9.0	128	8.1 + 5.8 = 13.9
L4-1R	70	91	…	82	3.3	119	4.3	114	8.0	125	6.7 + 5.6 = 12.3
L1-3R	101	110	2	119	4.8	168	6.5	152	7.4 + 7.1 = 14.5	191	8.2 + 10.7 = 18.9
L2-3R	100	104	…	109	4.5	139	6.3	148	7.8 + 4.0 = 11.8	150	8.5 + 7.5 = 16.0
L3-3R	82	93	…	83	4.1	128	5.7	120	5.8 + 4.0 = 9.8	131	5.9 + 7.4 = 13.3
L4-3R	81	92	…	82	3.4	125	5.0	119	5.2 + 3.4 = 8.6	127	5.5 + 4.7 = 10.2
L1-5R	105	110	2	130	7.3	181	7.7	167	9.5 + 7.3 = 16.8	197	6.3 + 12.5 = 18.8
L2-5R	95	106	…	117	6.3	141	7.2	147	8.1 + 6.7 = 14.7	157	5.4 + 9.8 = 15.2
L3-5R	84	97	…	115	4.8	134	6.6	129	5.0 + 7.5 = 12.5	138	5.9 + 8.9 = 14.8
L4-5R	83	96	…	112	4.6	132	5.6	121	4.0 + 6.9 = 10.9	132	7.5 + 5.3 = 12.8

Note: CN, nitride layer (compound layer + diffusion zone); CC + SC, compound layer + sublayer

80, 120, 240, 400, 600, 1000, and 1200 mesh, followed by polishing on 0.3 and 0.05 μm alumina abrasives, and ultrasonic cleaning in ethanol for 5 min. Etching with 2% nital (2% HNO_3-98% CH_3CH_2OH) revealed the microstructure. The micrographs were obtained with a Zeiss Axiotech optical microscope (Carl Zeiss, Basel, Switzerland) using differential interference contrast. For a more detailed analysis of the nitride layer microstructure, a Leo 440 (Carl Zeiss, Germany; Leica, U.K.) scanning electron microscope (SEM) operated at 33 kV was used. The SEM was equipped with an Oxford 7060 energy-dispersive x-ray spectrometer.

Microhardness measurements were carried out on a Micromet 2104 (Buehler, Ltd., IL) tester using a load of 50 gf. Five indentations were done in different locations on each sample surface. The thickness values for the nitrided layers were determined by measuring from the surface to the point where a hardness value 50 HV higher than the substrate value was achieved, according to the JIS G0562 standard (Ref 11).

X-ray diffraction (XRD) analyses were performed using a Rigaku Rotaflex (Rigaku Corporation, Tokyo, Japan) diffractometer with a Cu-Kα source ($\lambda = 0.15409$ nm) operated at 50 kV and 100 mA. The XRD measurements were performed with a time constant of 2 s, with a 2θ scan step of 2° per minute in the range of 30 to 120°.

The abrasive wear tests were done on a pin-on-disk wear machine using a 500-mesh SiC abrasive fixed onto a rotating disk. The sample, which also rotated, was fixed to an arm with a backward-and-forward movement that was pressed against a rotating disk, forming a spiral track on the abrasive paper. New abrasive paper was used for each test. Each sample was tested for 2000 turns, with a pause every 200 turns for mass loss measurements. At every pause, the sample was cleaned and weighed on a balance having a precision of 0.1 mg. A constant load of 320 g was applied to the sample, pressing it onto the rotating (53 rpm) abrasive paper. The wear tests were performed at room temperature without lu-

bricants, and the results were expressed in terms of the percent weight loss with respect to the initial weight (w_i) of the sample. These measurements (w_f) were taken for every 200 turns:

$$\text{Weight loss } (\%) = \frac{(w_i - w_f)}{w_i} \times 100 \quad \text{(Eq 1)}$$

3. Results and Discussion

The results of the chemical analysis of the alloys are presented in Table 2. Good agreement between these results and the nominal chemical compositions (Table 1) was obtained.

The Rockwell C hardness values for the quenched alloys were similar to those obtained before quenching (59-60 HRC). However, different hardness values were obtained after tempering (550 °C) for different treatment times. In Table 3, the effect of Si on the tempering of the alloys can be observed. The increase in the Si content helps to retard the rate of softening during tempering.

The influence of Si on this behavior can be due to the delay in the transformation of the ε carbide ($Fe_{2,4}C$) in either the η carbide (Fe_2C) (Ref 12) or in the more stable cementite (Fe_3C) (Ref 13). Si stabilizes the ε or η carbide, which can still be found in the microstructure of 1 to 2% Si steels after tempering at 400 °C, and at even higher temperatures for steels of higher Si content. The experimental results suggest that carbide nucleation and growth are retarded in the presence of Si, and that Si is part of the carbide structure. The martensite structure vanishes at about 300 °C for the carbon steels, but for the steels containing alloying elements, such as Cr, Mo, W, V, Ti, or Si, the tetragonal structure is still observed after tempering at 450 °C, and even at 500 °C. This means that these alloying elements enhance the stability of the supersaturated solid solution of Fe-C. On the contrary, Mn and Ni diminish this stability (Ref 12). For the L4 alloy, Mo can also influence the hardness. According to Krauss (Ref 13), this element retards the softening of the material during tempering. This effect is higher than the one for Si at a tempering temperature of 540 °C.

In Table 3, a decrease in the alloy hardness for longer tempering times was seen and is due to the transformation of the ε or η carbide into cementite, which, subsequently, coarsened with increased tempering time (Ref 13). The transition from ε or η carbide to cementite occurs by the nucleation of cementite in the interfaces between the ε and η carbides and the α-Fe matrix, followed by the dissolution of the metastable ε or η carbides (Ref 12).

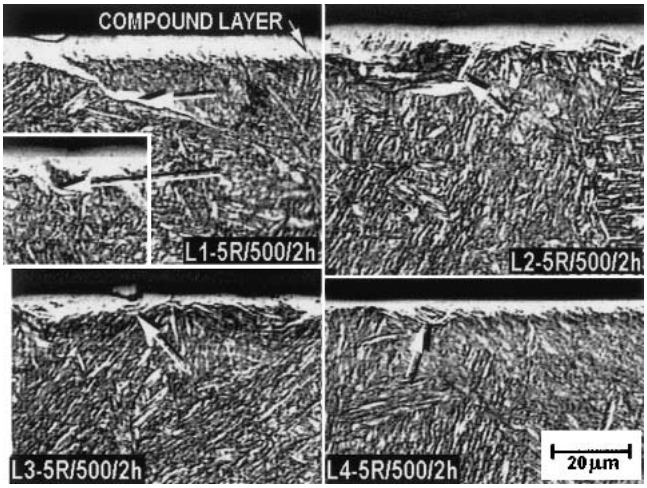

Fig. 3 Optical cross-sectional micrographs of the L1, L2, L3, and L4 alloys tempered for 5 h and ion nitrided at 500 °C for 2 h

3.1 Metallography and Microhardness

The ion-nitriding process demonstrated that a series of nitrided layers could be produced by varying the Si content, the treatment time, and temperature. Figure 1 displays the micrographs of the L1 (low Si content) and L4 (high Si content)

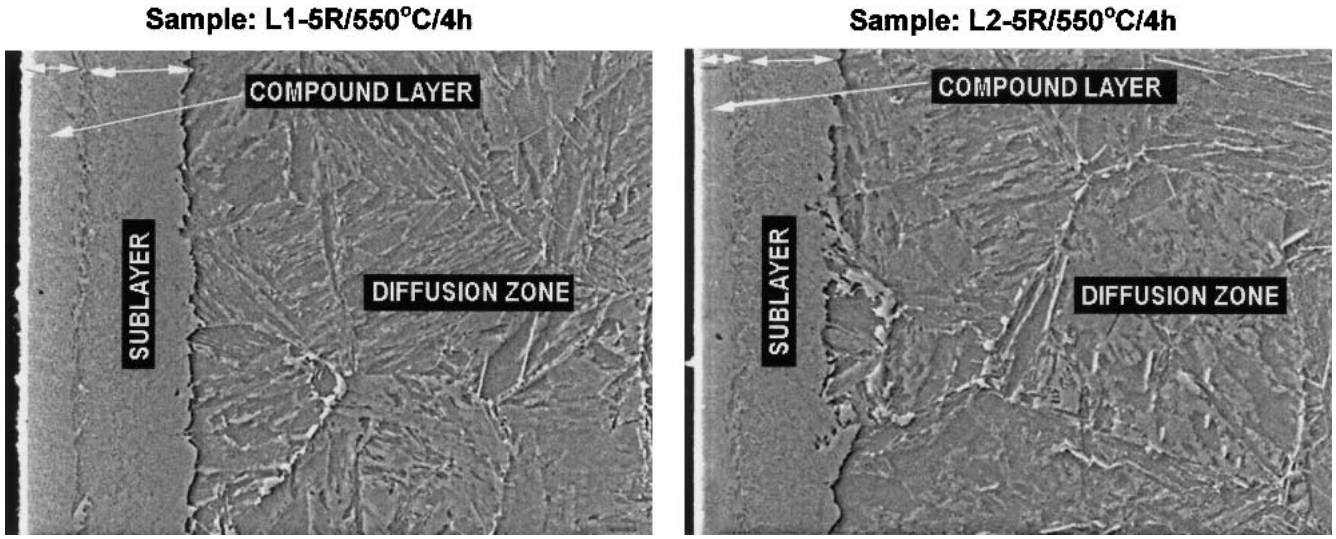

Fig. 4 SEM micrograph of the sublayer located between the compound layer and the diffusion zone for the L1 (left) and L2 (right) alloys tempered for 5 h and ion nitrided at 550 °C for 4 h

alloys, tempered for 5 h and nitrided at 350 °C for 4 and 8 h. The increase in the Si content caused a refinement in the martensite present in the substrate. The samples nitrided for 4 h show only a diffusion zone. A compound layer (indicated by arrows in Fig. 1) appeared in the L1 sample that had been nitrided for 8 h, but was not detected in the sample with higher Si content (L4). This indicates the need for times longer than 8 h or for higher temperatures for compound layer growth (Table 4). The diffusion zone cannot be visually distinguished from the martensitic matrix, being identified only by means of microhardness tests (Table 4).

The increase in temperature to 500 °C generated the formation of compound layers on the surfaces (Fig. 2, 3). These layers are constituted of nitrides, and their formation is a direct consequence of the high N gradient caused by sputtering at the plasma/surface interface. The compound layers are continuous and porosity-free, with projections toward the diffusion zone interior, and with preferential growth in the lath martensite boundaries (arrows in Fig. 2a). It can also be observed that the compound layer homogeneity is enhanced with treatment time (Fig. 2b), because N has enough time to diffuse. In Fig. 3, it should be noted that the thickness of the compound layer diminishes with the increase in Si in the alloy (Table 4), due probably to the increase in the N diffusion into the substrate interior caused by the presence of Si. According to the model of Köelbel (Ref 3, 14), the $Fe_2N \rightarrow Fe_3N \rightarrow Fe_4N$ transformation could be accelerated with the release of N, which could diffuse more easily into the substrate interior, making it difficult for the compound layer to grow. Also, regions with projections toward the diffusion zone interior are observed, probably due to N diffusion on the original austenitic grain boundaries.

The preferential sites of nitride formation are not well defined in the literature. Some authors have asserted that the nitrides are probably formed in the supersaturated matrix and on the grain boundaries. Others state that the nitrides are formed not only on the grain boundaries, but also inside the grains, due to the high level of N saturation. Edenhofer (Ref 15) observed preferential layer growth on some grain boundaries, and diffusion inside the grains after saturation, as is the case in the present work.

In the case of the samples nitrided at 550 °C for 2 and 4 h (Fig. 4), the presence of a sublayer is observed underneath the compound layer. The outer layer consists of a more compact nitride layer, because an initial deposition of Fe_2N nitride type occurred in it. Afterward, these nitrides lost N, which diffused into the alloy interior. An acceleration of the diffusion front probably occurred, and N transference from the outer compound layer was not able to recover the N below it, so that a N-deficient region formed with fewer nitrides. A thickness reduction was caused by the increase in the Si content in the alloy.

The influence of the Si content, time, and temperature on the surface hardness of the alloys, before and after ion nitriding, is shown in Fig. 5. It was observed that ion nitriding is an efficient process for enhancing the surface hardness of the quenched and tempered alloys. The surface hardness is a function of the nitriding temperature, because this temperature is important for the solubility and diffusion of N into the α-Fe matrix and for the kinetics.of nitride formation.

For the alloys nitrided at 350 °C, the highest surface hardness was obtained for 8 h of treatment. The N diffusion at low temperatures is slow. For the 8 h treatment, N had sufficient time to diffuse into the alloy, forming nitrides with the alloying elements, and consequently, increasing the hardness of the alloy. Comparing the microhardness values of samples nitrided at 350, 500, and 550 °C, a significant enhancement in the hardness with the increase in the temperature occurred. In this case, the influence of the treatment time was not considerable, and the increase in the hardness was due to the formation of the

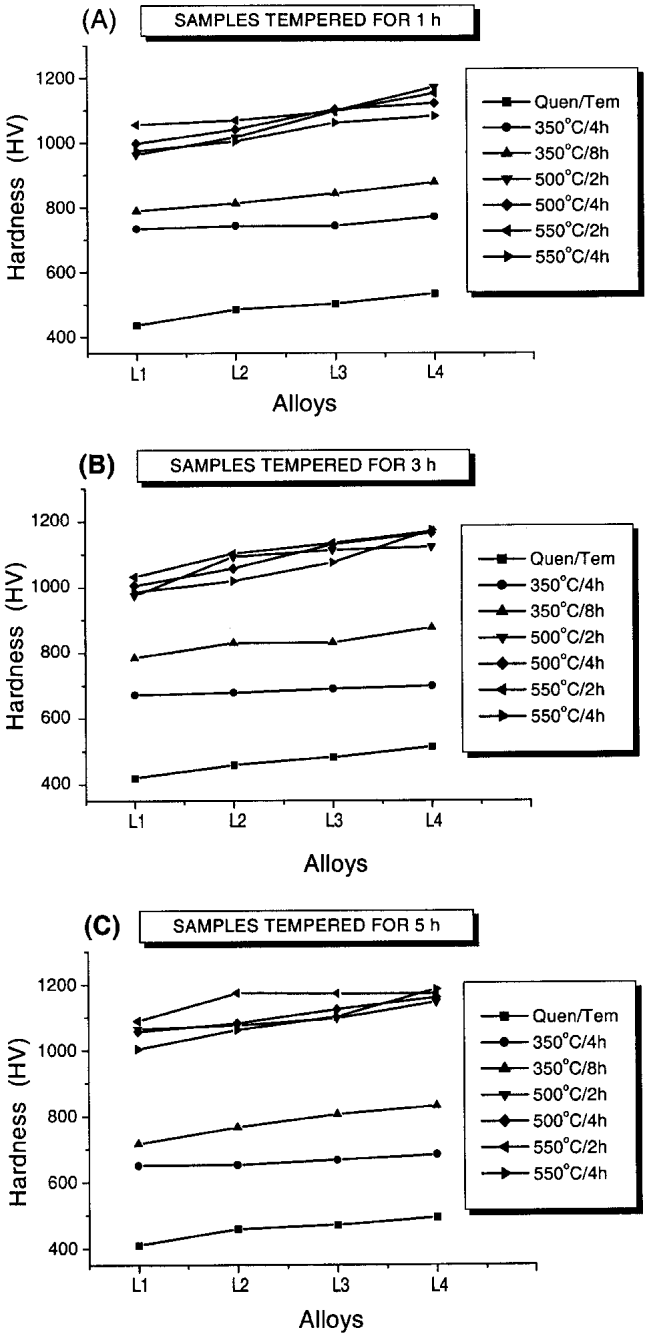

Fig. 5 Variation of the surface hardness of the L1, L2, L3, and L4 alloys before and after ion nitriding for different treatment conditions

compound layer, which was constituted by Fe and alloying element nitrides, such as Mo, Cr, and Si.

The alloy containing the least Si, L1 (0.62%), yielded the smallest surface hardness values. With increasing Si in the alloys L3 (1.68%) and L4 (1.98%), the hardness values increased, reaching 1185 HV for the L4 alloy. This can be attributed to the formation of a higher amount of Si nitride and also other element nitrides, such as Cr and Mo.

Because ion nitriding is a process that is related to diffusion, the increase in the treatment time and temperature (350, 500, and 550 °C) caused an increase in the thickness of the total nitrided layer (compound layer + diffusion zone) for all alloys. This behavior can be seen in Table 4.

The effects of tempering time, nitriding temperature, and Si content on the thickness of the nitrided layers are shown in Table 4. The layer thickness of the alloys nitrided at 500 °C

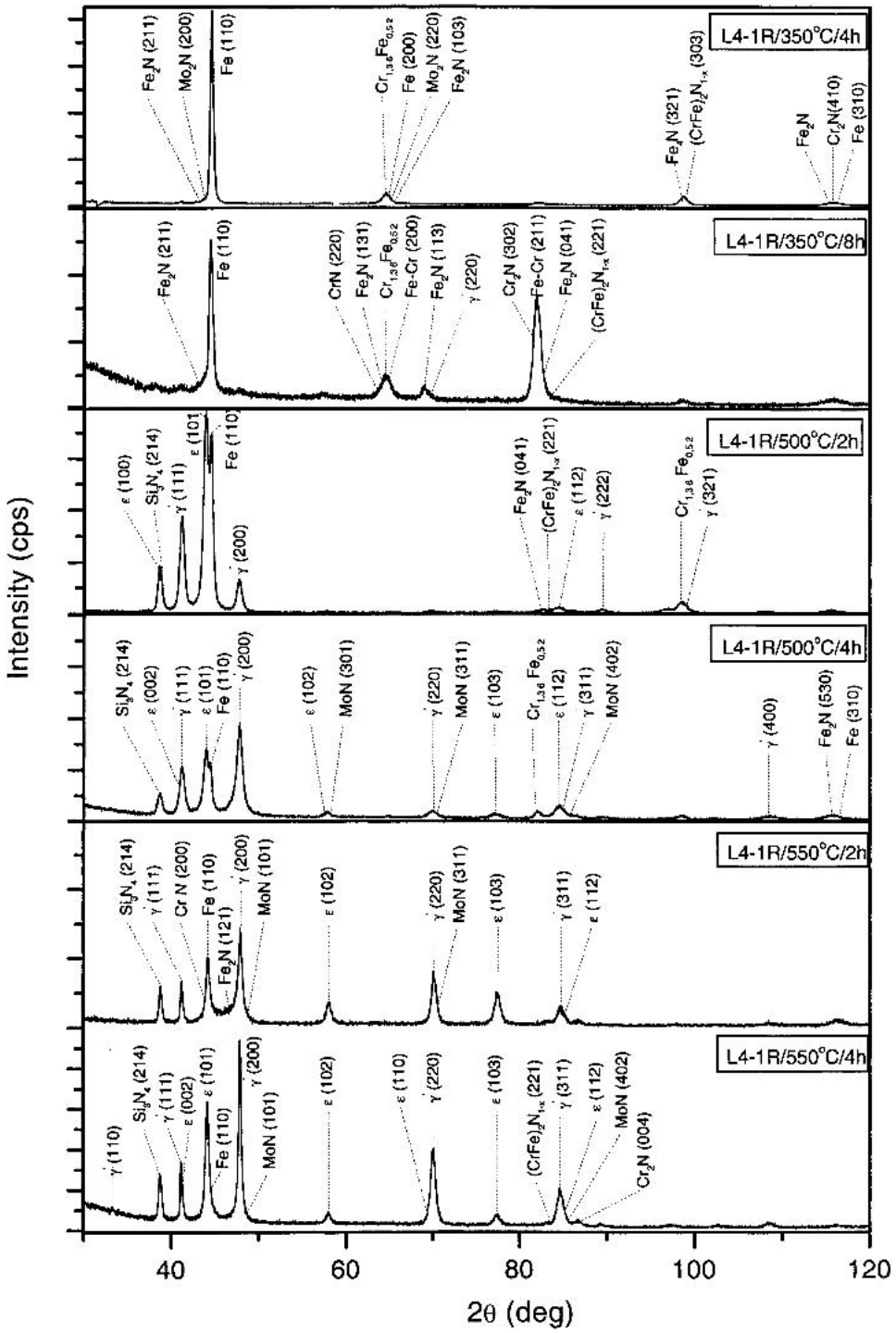

Fig. 6 X-ray diffractograms of the 1 h tempered L4 alloy nitrided at various temperatures and times

increased with 2 to 4 h of nitriding, but diminished with the increase in Si content. The increase in the tempering time also caused an increase in the compound-layer thickness, indicating that N diffusion occurred more easily after the martensite structure relaxed (i.e., with the formation of the ε or η carbides). For the samples nitrided at 550 °C, sublayers were also formed, and their thicknesses increased with nitriding time, but diminished with Si content. This thickness decrease was more pronounced in the sublayer than in the compound layer.

3.2 XRD

Figure 6 shows the diffractograms obtained for the different nitriding conditions, indicating that the nitride formation was influenced by the treatment time and temperature. For the nitriding treatment performed at 350 °C for 4 h, peaks associated with α-Fe, Fe_2N, Cr_2N, Mo_2N, and $(CrFe)_2N_{1-x}$ were identified. For the 8 h treatment, besides the aforementioned nitrides, γ'-Fe_4N and CrN were also detected.

The absence of γ' nitrides for the alloys treated for 4 h is probably due to the fact that in the N_2/H_2 plasma, the unstable Fe_2N initially forms on the surface, and its nonstability is caused by the supersaturation of N in the interstitial sites. This phase decomposes into more stable phases (e.g., γ'-Fe_4N and ε-$Fe_{2-3}N$) for longer treatment times, depending on the nitriding temperature (Ref 7). This corroborates the finding of Sun and Bell (Ref 16) that the γ' phase does not form in the beginning of the nitriding process, appearing only after some time. Metin and Inal (Ref 17) reported the presence of Fe_2N after 5 min of ion nitriding at 500 and 550 °C.

Increasing the ion nitriding temperature to 500 °C and 2 h of treatment caused the formation of a compound layer consisting of γ'-Fe_4N (predominant phase) and ε-$Fe_{2-3}N$, as well as small amounts of $(CrFe)_2N_{1-x}$ and Si_3N_4 (Fig. 6). The intensity of the γ' (200) peak, and the amount of the ε phase, increased with time (4 h), but the α(110) peak intensity diminished and the mixed nitride $(CrFe)_2N_{1-x}$ disappeared. The decrease in the α (110) peak intensity indicates that the compound layer thickness increased with nitriding time. The presence of the γ' and ε phases was also reported by Spalvins (Ref 18, 19).

The analysis of the diffractograms depicted in Fig. 6 for the samples nitrided at 550 °C for 2 and 4 h indicated the presence of MoN, CrN, Si_3N_4, γ'-Fe_4N, and ε-$Fe_{2-3}N$. A decrease in the Fe (110) peak intensity also occurred, with the subsequent appearance of extra ε peaks for the 4 h treatment.

The diffraction peak of the α-Fe, which is present in the diffusion zone (for the 350 °C nitriding temperature) and in the compound layer (for the 500 and 550 °C nitriding temperatures), was clearly observed for all samples, and its intensity diminished with the increase in time and treatment temperature, demonstrating the growth of the compound layer. The formation of $(CrFe)_2N_{1-x}$ nitride in the compound layer was due to the replacement of Fe atoms by Cr atoms in the nitrides, forming mixed nitrides, which have been observed by other authors (Ref 14, 20).

Comparing the diffractograms displayed in Fig. 6, it can be seen that the increase in the treatment time caused the formation of γ' and ε nitrides, with the quantity of each increasing with nitriding time.

3.3 Wear Testing

The thickness, hardness, and composition results of the nitrided layers helped to explain the abrasive wear behavior of the samples. Table 5 presents the mass loss results during the abrasive wear test and the surface hardness values for the all samples under different conditions. The mass losses of the nitrided alloys are smaller than those of the nonnitrided (i.e., quenched-and-tempered) alloys, demonstrating the effectiveness of the nitriding treatment in enhancing wear resistance. The samples nitrided at 350 °C for 8 h presented a slight improvement in the wear performance in comparison with the samples treated for 4 h. This better performance is related to the increase in hardness and the formation of nitrides such as CrN and Fe_4N (Fig. 6). For the samples nitrided at 500 and 550 °C for 2 and 4 h, smaller mass losses occurred for the samples treated for 2 h, because the compound layers of these

Table 5 Surface hardness and mass loss results for the nonnitrided and nitrided samples

			Ion nitriding											
	Heat treatment		350 °C 4 h		350 °C 8 h		500 °C 2 h		500 °C 4 h		550 °C 2 h		550 °C 4 h	
Alloy	HV	ML, %	HV	ML, %	HV	ML, %	HV	ML, %	HV	ML, %	HV	ML, %	HV	ML, %
L1-1R	436	86	734	63	784	49	963	39	998	41	1055	39	975	41
L2-1R	481	79	743	57	813	44	1017	37	1041	40	1069	38	1004	40
L3-1R	500	71	743	56	843	33	1098	36	1104	40	1096	37	1062	40
L4-1R	534	69	772	49	878	29	1173	34	1123	39	1154	36	1083	38
L1-3R	419	82	672	59	780	50	975	40	1005	40	1032	41	985	41
L2-3R	459	76	678	54	830	48	1092	39	1057	38	1103	40	1019	41
L3-3R	482	73	690	50	831	47	1113	39	1130	38	1134	37	1075	40
L4-3R	502	69	698	45	876	44	1123	37	1165	38	1170	37	1174	39
L1-5R	404	86	650	52	716	52	1065	41	1057	40	1089	41	1004	39
L2-5R	458	74	652	52	766	52	1076	36	1082	39	1174	36	1062	39
L3-5R	470	74	666	50	805	50	1097	36	1124	39	1172	36	1102	37
L4-5R	493	71	682	47	830	47	1146	35	1160	38	1172	35	1185	37

HV, Vickers hardness; ML, mass loss

samples were constituted by CrN and γ'-Fe_4N phases, which are more ductile and wear resistant than the other phases.

The compound layer thickness also affected the wear behavior of the nitrided alloys, as can be seen in Tables 4 and 5. The thicker compound layer of the L1 alloy resulted in higher mass loss compared with the L4 alloy, which had a thinner compound layer. This behavior was observed by Karamis (Ref 21), who reported that the wear rate increased for alloys with a thicker compound layer, for dry-sliding conditions, and that this wear rate was related to compound layer spalling. The reason for this spalling could be the presence of γ' and ε phases in the same proportions in the compound layer. The presence of mixed nitrides produces weak interface boundaries because they have different crystallographic cells, causing a growth mismatch that results in brittleness. Besides this, the increase in wear can also be due to the entrapment of hard abrasive particles, produced by the compound layer fracture during the initial step of sliding (Ref 22).

The increase in the Si content not only influenced the compound layer thickness but also caused an increase in the surface hardness and abrasive wear resistance of the layers (Table 5). Similar findings were reported by Klein et al. (Ref 23) and Maliska et al. (Ref 24) for nitrided Fe-based materials.

The results summarized in Table 5 also showed the classic

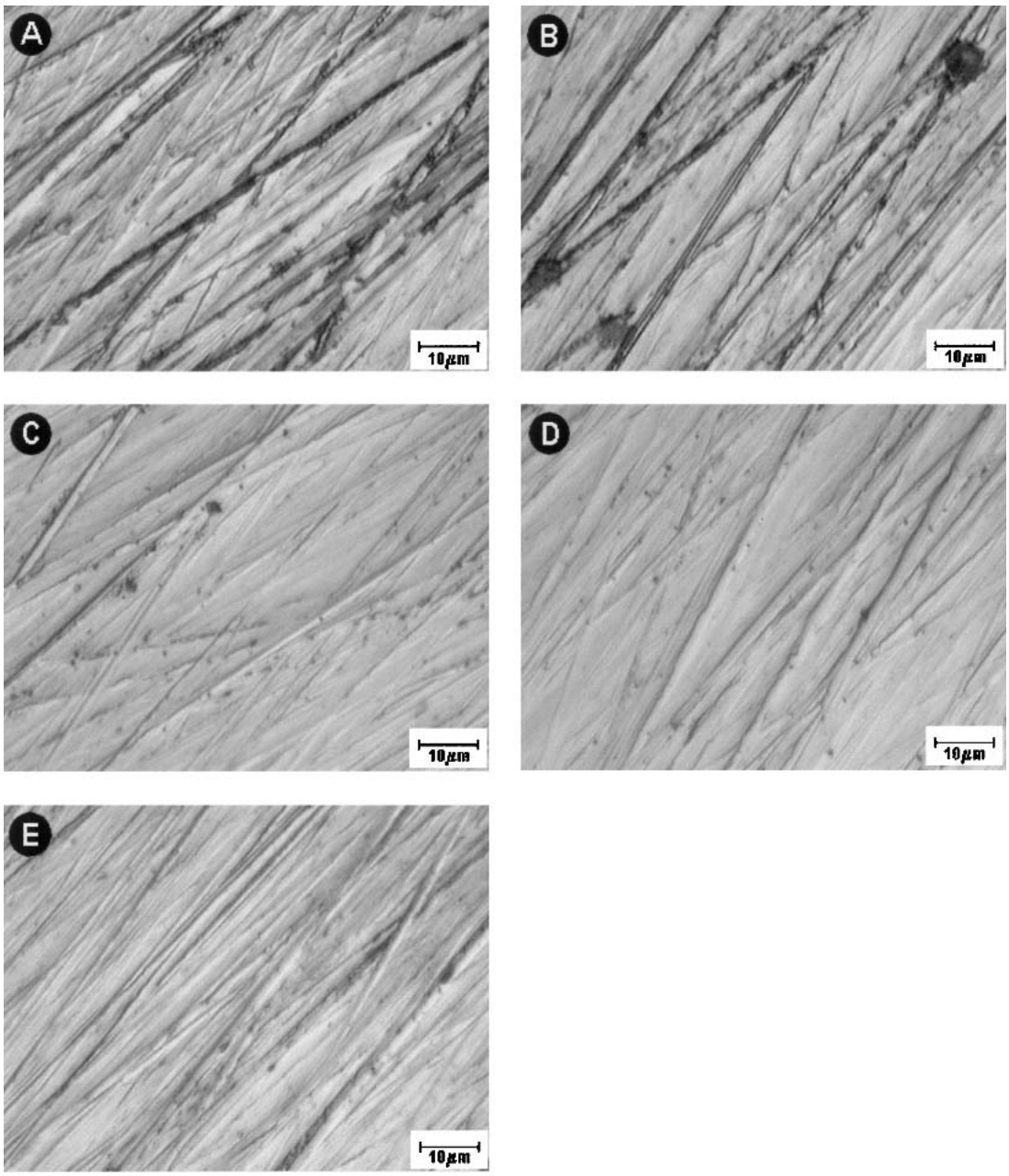

Fig. 7 Optical micrographs of the worn surfaces of the nonnitrided and nitrided samples. (a) L1-1R. (b) L4-5R. (c) L4-1R/500 °C/2 h (least mass loss). (d) L4-3R/500 °C/4 h. and (e) L1-1R/500 °C/4 h (highest mass loss)

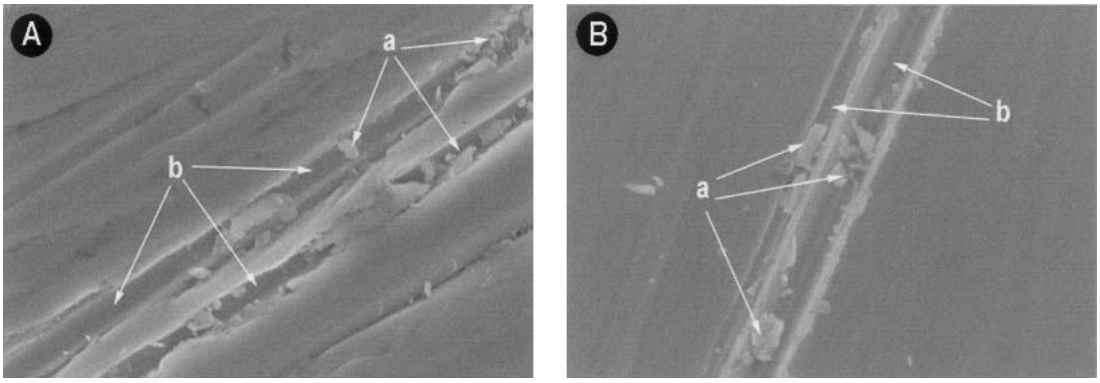

Fig. 8 SEM micrographs of the worn L2 alloy tempered for 1 h and ion nitrided at 350 °C for (a) 4 h and (b) 8 h

correlation between the decrease in wear and the increase in surface hardness. The highest wear rate was exhibited by the L1 alloy, which possessed the lowest surface hardness and the thickest compound layers. The L4 alloy with smaller wear rates had the highest surface hardness and the thinnest compound layers.

The optical micrographs of the worn surfaces of the 4340M alloys are shown in Fig. 7. The worn surfaces of the nonnitrided alloys correspond to the L1-1R alloy (Fig. 7a) and the L4-5R alloy (Fig. 7b), which yielded the highest and the smallest mass losses, respectively, and the nitrided alloys (Fig. 7c-e), which possessed the best, intermediate, and the worst abrasive wear behavior.

After the wear tests, the nonnitrided alloy surfaces exhibited the typical microstructural aspects of abrasive wear (Fig. 7a, b). Material removal occurred through deep and wide grooving in the sliding direction. The groove depth and width are smaller for the nitrided samples (Fig. 7c, d). In the surface topographies of the nitrided samples, mainly those that achieved better wear performance, mild wear was observed, which produced an almost polished surface, with a slight and homogeneous tracking in the movement direction and a surface smoothing (Fig. 7c, L4-1R/500 °C/2 h). This behavior was caused probably by the formation of a two-phase layer of γ' and ε nitrides, with a predominance of the γ' phase, demonstrating that compound layers formed by these phases have good wear resistance. Both the γ' and ε phases have good ductility despite its high hardness, and this is, perhaps, one of the reasons for the ability of the compound layer to resist grooving, leading to lower mass loss. The aspect of the nitrided alloy surface that presented the highest mass loss was probably due to the removal of the compound layer, and the observed rough tracks were, in fact, related to the substrate.

Figure 8 displays the SEM micrographs of the worn surfaces of the samples nitrided at 350 °C. Significantly higher damage in the sample was observed for the alloy nitrided for 4 h compared with the one nitrided for 8 h, although the damaged regions present similar microstructural aspects. Probably, microparticles were initially detached from the surface (arrow, a) or from the abrasive paper, and this then caused grooving (arrow, b). The best wear performance of the L1-1R/350 °C/8 h could be related to the formation of nitrides such as Mo_2N, $(CrFe)_2N_{1-x}$, Fe_2N, and Fe_4N.

4. Conclusions

By changing the Si content in the ion-nitriding process, a variety of nitrided layers were produced depending on treatment time and temperature. The increase in Si content in the alloys enhanced their tempering resistance and also improved considerably the hardness of the nitrided layers. XRD detected a mixture of nitrides (i.e., γ'-Fe_4N, ε-$Fe_{2-3}N$, CrN, MoN, and Si_3N_4) with their proportions varying with the nitriding conditions. The ion-nitriding process improved the abrasive wear resistance of the alloys. The increase in Si also produced thinner compound layers with the highest hardness and best abrasive wear resistance.

Acknowledgment

This work was supported by FAPESP, CAPES, and CNPq of Brazil.

References

1. T.V. Philip, Ultrahigh Strength Steels, *Properties and Selection: Irons, Steels, and High-Performance Alloys,* Vol 1, *ASM Handbook,* ASM International, 1990, p 424
2. B. Edenhofer, Physical and Metallurgical Aspects of Ionitriding: Part 1, *Heat Treat. Met.,* Vol 1, 1974, p 23-28
3. J. O'Brien and D. Goodman, Plasma (Ion) Nitriding, *Heat Treating,* Vol 4, *ASM Handbook,* ASM International, 1991, p 420-424
4. C.K. Jones, S.W. Martín, and M. Hudis, "Ion Nitriding," Proc. Conf. on Heat Treatment (London, U.K.), The Metals Society, 1973, p 71-77
5. W. Rembges, Fundamentals, Applications and Economical Considerations of Plasma Nitriding, *Conference on Ion Nitriding* (Cleveland, OH), ASM International, 1986, p 189-198
6. B. Edenhofer, Low Temperature Ion-Nitriding: Nitriding at Temperatures Below 500°C for Tools and Precision Machine Parts, *Proc. Conf. on Heat Treatment 73* (London, U.K.), Vol 12-13, The Metals Society, 1973, p 7
7. O.T. Inal, K. Ozbaysal, E.S. Metin, and N.Y. Pehlinvanturk, A Review of Plasma Surface Modification Process, Parameters, and Microstructural Characterization, *Proc. Second Int. Conf. on Ion Nitriding/Carburizing* (Cincinnati, OH), ASM International, Sept 1989, p 57-66
8. K.H. Jack, Nitriding, *Proc. Conf. on Heat Treatment 73* (London, U.K.), The Metals Society, 1973, p 39-50
9. T. Spalvis, Advances and Directions of Ion Nitriding/Carburizing, *Proc. Second Int. Conf. on Ion Nitriding/Carburizing* (Cincinnati, OH), Sept 1989, p 1-4
10. "Standard Specification for Castings, Steel and Alloy, Common Re-

quirements for General Industrial Use," A 781/A 781M-92, *Annual Book of ASTM Standards,* ASM International, p 421
11. Japanese Industrial Standard JIS G0562, Method of Measuring Nitrided Case Depth for Iron and Steel, *Surf. Eng.,* Vol 11 (No. 1), 1995, p 57-60
12. Y. Hirotsu and S. Nagakura, Crystal Structure and Morphology of the Carbide Precipitated from Martensite High Carbon Steel During the First Stage of Tempered, *Acta Met.*, Vol 20, 1972, p 645-655
13. G. Krauss, *Steels: Heat Treatment and Processing Principles,* ASM International, 1990
14. K.H. Jack, The Effect of Substitutional Alloying Elements on the Behaviour Of Interstitial Solutes In Iron, *Scand. J. Metall.,* Vol 1, 1972, p 195-202
15. B. Edenhofer, Physical and Metallurgical Aspects of Ionitriding: Part 2, *Heat Treat. Met.,* Vol 2, 1974, p 59-67
16. Y. Sun and T. Bell, Computer Prediction of Threshold Nitriding Potential Curves, *Heat Treat. Met.,* Vol 2, 1997, p 43-49
17. E. Metin and O.T. Inal, Formation and Growth of Iron Nitrides During Ion-Nitriding, *J. Mater. Sci.,* Vol 22, 1987, p 2783-2788
18. T. Spalvins, Tribological and Microstructural Characteristics of Ion-Nitrided Steel, *Proc. Int. Conf. on Metallurgical Coatings* (San Diego, CA), ASC International, 1983, p 157-163
19. T. Spalvins, Frictional and Structural Characterization of Ion-Nitrited Low and High Chromium Steels, *J. Vac. Sci. Technol.,* Vol A3 (No. 6), 1985, p 2329-2333
20. D.H. Jack and K.H. Jack, Invited Review: Carbides and Nitrides in Steel, *Mater. Sci. Eng.,* Vol 11, 1973, p 1-27
21. M.B. Karamis, An Investigation of the Properties and Wear Behavior of Plasma-Nitrided Hot Working Steel (H13), *Wear,* Vol 150, 1991, p 331-342
22. B. Podgornik, J. Vizintin, and V. Leskovsek, Tribological Properties of Plasma and Pulse Plasma Nitrided AISI 4140 Steel, *Surf. Coat. Technol.,* Vol 108-109, 1998, p 454-460
23. A.N. Klein, R. Oberacker, and F. Thummler, High Strength Si-Mn Alloyed Sintered Steels, *Powder Metall. Int.,* Vol 17, 1987, p 13-16
24. A.M. Maliska, A.N. Klein, and A.R. Souza, Microestructural Characterization of Plasma Nitriding Surface of Sintered Steels Containing Si, *Surf. Coat. Technol.,* Vol 70, 1995, p 175-179